WL-TR-91-3098

AD-A244 320

COMPUTATION OF A KELVIN-HELMHOLTZ INSTABILITY
FOR DELTA WING VORTEX FLOWS

Raymond E. Gordnier
MicroCraft Inc.
207 Big Springs Avenue
PO Box 370
Tullahoma, TN 37388-0370

November 1991

Final Report for Period 1 September 1990 - 1 September 1991

DTIC
ELECTE
JAN 14 1992
S   B   D

FLIGHT DYNAMICS DIRECTORATE
WRIGHT LABORATORY
AIR FORCE SYSTEMS COMMAND
WRIGHT-PATTERSON AIR FORCE BASE, OHIO 45433-6553

92-01154

02 1 13 063

NOTICE

When Government drawings, specifications, or other data are used for any purpose other than in connection with a definitely Government-related procurement, the United States Government incurs no responsibility nor any obligation whatsoever. The fact that the government may have formulated, or in any way supplied the said drawings, specifications, or other data, is not to be regarded by implication or otherwise in any manner construed, as licensing the holder or any other person or corporation, or as conveying any rights or permission to manufacture, use, or sell any patented invention that may in any way be related thereto.
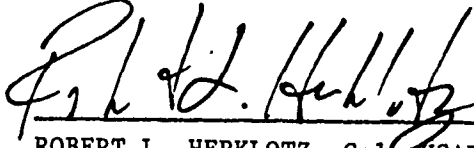
This report is releasable to the National Technical Information Service (NTIS). At NTIS, it will be available to the general public, including foreign nations.

This technical report has been reviewed and is approved for publication.

RAYMOND E. GORDNIER
Visiting Scientist

JOSEPH J. S. SHANG, Tech Mgr
Computational Aerodynamic Group

FOR THE COMMANDER

ROBERT L. HERKLOTZ, Col, USAF
Chief
Aeromechanics Division

REPORT DOCUMENTATION PAGE

Public reporting burden for this collection of information is estimated to average 1 hour per response, including the time for reviewing instructions, searching existing data sources, gathering and maintaining the data needed, and completing and reviewing the collection of information. Send comments regarding this burden estimate or any other aspect of this collection of information, including suggestions for reducing this burden to Washington Headquarters Services, Directorate for Information Operations and Reports, 1215 Jefferson Davis Highway, Suite 1204, Arlington, VA 22202-4302, and to the Office of Management and Budget, Paperwork Reduction Project (0704-0188), Washington, DC 20503

1. AGENCY USE ONLY (Leave blank)	2. REPORT DATE	3. REPORT TYPE AND DATES COVERED
	5 Nov 91	Final Report, 1 Sep 90 – 1 Sep 91

4. TITLE AND SUBTITLE	5. FUNDING NUMBERS
Computation of a Kelvin-Helmholtz Instability for Delta Wing Vortex Flows	(C) F33601-89-D0045 (PE) 61102F (PR) 2307

6. AUTHOR(S)

Raymond E. Gordnier

(TA) N6
(WU) 11

7. PERFORMING ORGANIZATION NAME(S) AND ADDRESS(ES)	8. PERFORMING ORGANIZATION REPORT NUMBER
Micro Craft, Inc 207 Big Springs Avenue PO Box 370 Tullahoma TN 37388-0370	

9. SPONSORING/MONITORING AGENCY NAME(S) AND ADDRESS(ES)	10. SPONSORING/MONITORING AGENCY REPORT NUMBER
Joseph J. S. Shang, (513) 255-7127 Flight Dynamics Directorate (WL/FIMM) Wright Laboratory Air Force Systems Command Wright-Patterson AFB OH 45433-6553	WL-TR-91-3098

11. SUPPLEMENTARY NOTES

12a. DISTRIBUTION/AVAILABILITY STATEMENT

Approved for public release; distribution is unlimited

12b. DISTRIBUTION CODE

13. ABSTRACT (Maximum 200 words)

The structure of the shear layer which emanates from the leading edge of a 76 degrees sweep delta wing and forms the primary vortex is investigated numerically. The flow conditions are $M\infty = 0.2$, Re = 50,000 and angle of attack of 20.5 degrees. Computational results are obtained using a Beam-Warming type algorithm. The existence of a Kelvin-Helmholtz type instability of the shear layer which emanates from the leading edge of the delta wing is demonstrated. A description is provided of the three-dimensional, unsteady behavior of the small-scale vortices associated with this instability. The numerical results are compared qualitatively with experimental flow visualizations exhibiting similar behavior.

14. SUBJECT TERMS			15. NUMBER OF PAGES
Delta Wing, Vortical Flow, Kelvin-Helmholtz Instability			36
			16. PRICE CODE

17. SECURITY CLASSIFICATION OF REPORT	18. SECURITY CLASSIFICATION OF THIS PAGE	19. SECURITY CLASSIFICATION OF ABSTRACT	20. LIMITATION OF ABSTRACT
Unclassified	Unclassified	Unclassified	UL

Table of Contents

List of Figures

iv

Acknowledgement

1. Introduction

Enhancement of the maneuverability and controllability of current and future fighter aircraft requires the ability to more accurately predict the aerodynamics of these vehicles during rapid maneuvers and at the extremes of their flight envelopes. This has led to a particular interest in high angle of attack and unsteady aerodynamics. One of the dominant features of the flow field around a fighter aircraft at angle of attack is the vortex flow above the delta wing. A better understanding of this flow field will lead to an improved understanding of the aerodynamics of a fighter aircraft. The vortex flow over a delta wing also provides a good model for studying complex, three-dimensional vortical flows. This work is part of a continuing effort to improve predictive capabilities for both high angle of attack and unsteady aerodynamics.

The present work has developed out of a series of experimental and computational investigations of the following background. Gad-el-Hak and Blackwelder [1] observed for water tunnel tests of two delta wings that the vortex sheet which emanates from the leading edge of the delta wing rolls up into discrete vortices that undergo a pairing process. The instability appears as alternating dark and light regions in the dye sheet near the leading edge of the delta wing and extending along it, figure 1. This instability is said to be similar to the instability and pairing process described by Brown and Roshko [2] and Winant and Browand [3] for two-dimensional shear layers. Both are related to the classical Kelvin-Helmholtz type instability of two-dimensional shear layers.

Payne *et al.* [4] also observed an instability in the shear layer forming the primary vortex using smoke flow visualization techniques. They again relate the growth of these secondary structures to the classical Kelvin-Helmholtz type of instability. The observed vortical structures appeared to be static, however, and did not rotate with the vortex. They relate these observations [5] to those of Gad-el-Hak and Blackwelder.

Lowson [6] has carried out low speed wind tunnel tests to investigate the vortex sheet structure formed about delta wings. In this work he concludes that not one, but two types of instability exist in the shear layer leaving the leading edge. The first, shown in figure 2 is the quasi two-dimensional type of instability observed by Gad-el-Hak. The second is a locally streamwise instability of the vortex sheet that gives rise to steady structures within the vortex core. Lowson suggests that this is the instability observed by Payne *et al.*

All these experimental results have been obtained for scaled models at relatively low Reynolds number. Recent photographic evidence shows that similar types of secondary vortical structures are observed for the LEX vortex flow on an F-18 in flight [7]. This strongly indicates that the vortex structure found experimentally at lower Reynolds number occurs in flight conditions at full scale Reynolds number.

A similar type of shear-layer instability was observed by the present authors [8] in calculations for a 76° sweep delta wing at 20.5° angle of attack and a Reynolds number of 900,000. An unsteady behavior of the shear layer which emanates from the leading edge of the delta wing, related to the instability described by Gad-el Hak and Blackwelder, was found in these calculations. Uncertainties in the effect of grid resolution, temporal accuracy, and Reynolds number were noted.

The current work addresses some of the uncertainties noted for the previous work. Further computations are performed at a lower Reynolds number, $Re = 50,000$, and for enhanced grid resolution. An improved description of the unsteady process observed will be given. The lower values of Reynolds number will also provide the ability to more closely relate the numerical results to the existing experimental observations just described.

2. Governing Equations

The governing equations for the present problem are the unsteady, three-dimensional, full Navier-Stokes equations written in strong conservation form [9] using a general coordinate transformation ξ, η, ζ, t:

$$\frac{\partial}{\partial t}\left(\frac{q}{J}\right) + \frac{\partial F}{\partial \xi} + \frac{\partial G}{\partial \eta} + \frac{\partial H}{\partial \zeta} = \frac{1}{Re}[\frac{\partial \dot{F}_v}{\partial \xi} + \frac{\partial G_v}{\partial \eta} + \frac{\partial H_v}{\partial \zeta}] \tag{2.1}$$

where

$$q = \begin{bmatrix} \rho \\ \rho u \\ \rho v \\ \rho w \\ \rho E_t \end{bmatrix}, \quad F = \frac{1}{J}\begin{bmatrix} \rho U \\ \rho u U + \xi_x p \\ \rho v U + \xi_y p \\ \rho w U + \xi_z p \\ \rho E_t U + p\tilde{U} \end{bmatrix}, \quad G = \frac{1}{J}\begin{bmatrix} \rho V \\ \rho u V + \eta_x p \\ \rho v V + \eta_y p \\ \rho w V + \eta_z p \\ \rho E_t V + p\tilde{V} \end{bmatrix}, \quad H = \frac{1}{J}\begin{bmatrix} \rho W \\ \rho u W + \zeta_x p \\ \rho v W + \zeta_y p \\ \rho w W + \zeta_z p \\ \rho E_t W + p\tilde{W} \end{bmatrix},$$

$$F_v = \frac{1}{J}\begin{bmatrix} 0 \\ \xi_x \tau_{i1} \\ \xi_x \tau_{i2} \\ \xi_x \tau_{i3} \\ \xi_x b_i \end{bmatrix}, \quad G_v = \frac{1}{J}\begin{bmatrix} 0 \\ \eta_x \tau_{i1} \\ \eta_x \tau_{i2} \\ \eta_x \tau_{i3} \\ \eta_x b_i \end{bmatrix}, \quad H_v = \frac{1}{J}\begin{bmatrix} 0 \\ \zeta_x \tau_{i1} \\ \zeta_x \tau_{i2} \\ \zeta_x \tau_{i3} \\ \zeta_x b_i \end{bmatrix}$$

$$U = \xi_t + \xi_x u + \xi_y v + \xi_z w = \xi_t + \tilde{U}$$

$$V = \eta_t + \eta_x u + \eta_y v + \eta_z w = \eta_t + \tilde{V}$$

$$W = \zeta_t + \zeta_x u + \zeta_y v + \zeta_z w = \zeta_t + \tilde{W}$$

$$E_t = e + \frac{1}{2}(u^2 + v^2 + w^2)$$

$$b_i = u_j \tau_{ij} + \frac{k}{(\gamma - 1)PrM_\infty^2}\frac{\partial T}{\partial x_i}$$

$$\tau_{ij} = \mu(\frac{\partial \xi_k}{\partial x_j}\frac{\partial u_i}{\partial \xi_k} + \frac{\partial \xi_k}{\partial x_i}\frac{\partial u_j}{\partial \xi_k}) - \frac{2}{3}\mu\delta_{ij}\frac{\partial \xi_l}{\partial x_k}\frac{\partial u_k}{\partial \xi_l}$$

$$x_1, x_2, x_3 - x, y, z$$

The system of equations is closed using the perfect gas law, Sutherland's formula for viscosity, and the assumption of a constant Prandtl number, $Pr = 0.72$. Flow quantities have been nondimensionalized by their respective free stream values except for pressure, which is nondimensionalized by twice the freestream dynamic pressure, and speed of sound which is nondimensionalized by the freestream velocity. All lengths have been normalized by the root chord length of the delta wing.

3

3. Numerical Procedure

The governing equations are solved numerically using the implicit approximately factored algorithm of Beam-Warming [10]. The equations are differenced using Euler implicit time-differencing and second-order accurate central differences for all spatial derivatives. A blend of second and fourth order nonlinear dissipation, as suggested by Jameson [11], is used to stabilize the central difference scheme. The current work, in which subsonic flows are investigated, requires only fourth-order dissipation.

A fully vectorized, time-accurate solver has been developed to implement the aforementioned scheme [12]. The computational requirements of the scheme are approximately 38 words/grid point and 4.4×10^{-5} CPU sec/grid point/iteration on a Cray 2. This code has been validated for a number of simple laminar flows. Solutions for the case of a supersonic delta wing have been compared with both experimental results and other numerical results [13]. Good agreement for both comparisons has been obtained. The code has also been shown to capture successfully transition from Couette flow to Taylor-vortex flow due to centrifugal instability [12]. Unsteady results have been obtained for a pitching slender body of revolution [14]. Finally, the code has been used to calculate both steady and unsteady horseshoe vortex flows occurring at a cylinder/flat plate juncture [15]. These results have provided a good validation base for the code. It is of particular importance that the latter results demonstrate the ability to correctly simulate naturally occurring instabilities in the flow field and the transition of the flow from steady to unsteady behavior.

MacCormack[16] suggests that a desirable form of a numerical method is:

$$\{numerics\}\Delta q = \{physics\} \tag{3.1}$$

This form allows modifications to the left-hand side of equation (3.1) for numerical reasons (e.g., efficiency) without affecting the accurate representation of the governing physical equations contained on the right-hand side. The current numerical procedure has this form for steady flows. Implementing a Newton-like subiteration procedure recovers this form for unsteady flows. This subiteration procedure has been successfully used by several authors [17,18,19]. The Newton subiteration procedure can provide distinct improvements to the current numerical scheme. Subiteration improves the accuracy of the scheme via reduction or elimination of both factorization and linearization errors. Relaxation of stability limits in the three-factored scheme due to the reduction of the factorization error improves the efficiency of the scheme. Finally, one may obtain higher-order temporal accuracy in a straightforward fashion.

The subiteration procedure is implemented in the currently existing code with a few simple modifica-

4

tions. The standard Beam-Warming algorithm for equation (2.1) is written as follows:

$$[\frac{I}{J^{n+1}} + \Delta t L_\xi]J^{n+1}[\frac{I}{J^{n+1}} + \Delta t L_\eta]J^{n+1}[\frac{I}{J^{n+1}} + \Delta t L_\zeta]\Delta q^n = -\Delta t \dot{R}^n \tag{3.2}$$

with:

$$\dot{R}^n = \delta_\xi F + \delta_\eta G + \delta_\zeta H - \frac{1}{Re}[\delta_\xi F_v + \delta_\eta G_v + \delta_\zeta H_v]$$

$$\Delta q^n = q^{n+1} - q^n$$

$$L_\xi = \delta_\xi(\dot{A} + Q_{1\xi})$$

$$L_\eta = \delta_\eta(B + Q_{2\eta})$$

$$L_\zeta = \delta_\zeta(C + Q_{3\zeta})$$

where $A, B,$ and C are the inviscid flux Jacobians and $\dot{Q}_1, \dot{Q}_2,$ and Q_3 are the appropriate viscous flux Jacobians. For the subiteration procedure one term is added to the right hand side of equation (3.2) and the definition of Δq^n is modified, yielding:

$$[\frac{I}{J^{n+1}} + \Delta t L_\xi]J^{n+1}[\frac{I}{J^{n+1}} + \Delta t L_\eta]J^{n+1}[\frac{I}{J^{n+1}} + \Delta t L_\zeta]\Delta q^p = -\Delta t_s[\frac{q^p - q^n}{\Delta t_{phy}} + \dot{R}^p] \tag{3.3}$$

where:

$$\dot{q} = q/J$$

$$\Delta q^p = q^{p+1} - q^p$$

$$\Delta t_s = \text{subiteration time step}$$

$$\Delta t_{phy} = \text{physical time step.}$$

Here p is the subiteration count. For $p = 0$, $q^p = q^n$ and the scheme reverts to the noniterative form of the algorithm, equation (3.2). As $p \to \infty$, $q^p \to q^{n+1}$ and the solution at the new time level is obtained.

Currently, the subiteration procedure is implemented using the same factorization scheme as the noniterative algorithm. Since the physics of the problem now is contained in the right-hand side of equation (3.3), the left-hand side may be modified to improve the efficiency of the numerical scheme without adversely affecting the time accuracy of the problem. This area remains for future investigation.

5

4. Grid Structure and Boundary Conditions

The computational grid for the delta wing was obtained using simple algebraic grid generation techniques. The grid structure is of an H-H type with planar grids being stacked in the axial direction. The H-H structure provides for good resolution of the sharp leading edge with no rounding. All farfield boundaries are located 1.5 to 2 chord lengths away from the delta wing. The grid configuration is shown in figure 4.

The boundary conditions are implemented in the following manner. On the wing surface, the no-slip condition for the velocities, adiabatic wall temperature condition and zero normal pressure gradient condition are used. At the downstream boundary, flow variables are extrapolated from the interior. This allows for convection of the vortices out of the computational domain. Symmetry conditions are imposed along the mid-plane of the wing.

Characteristic boundary conditions [20] are used at the upper, lower, side, and upstream boundaries. Locally one-dimensional flow is assumed from which the corresponding characteristic variables are obtained. The boundary conditions are then applied to the characteristic variables with their values being specified from either the freestream or interior values depending on the sign of the corresponding eigenvalue. For subsonic inflow four characteristic variables are specified from the freestream conditions with the fifth extrapolated from the interior. For subsonic outflow four characteristic variables are specified from the interior with one variable specified from the freestream values. In the present calculations, the upstream and lower boundaries are inflow boundaries, and the upper and side boundaries are outflow boundaries. The specification of characteristic conditions reduce undesirable reflections from the boundaries of the computational domain.

5. Results

5.1 High Reynolds Number Case

All results presented are calculated for a 76° sweep delta wing of aspect ratio 1 (fig. 3). This configuration has been investigated experimentally by Hummel [21,22]. The first calculations for this configuration [8] are made at Reynolds number 900,000, angle of attack of 20.5°, and a freestream Mach number 0.2. These conditions correspond to the experiment of Hummel, except for the Mach number which is higher than the experimental Mach number, 0.05. A node system consisting of $66 \times 151 \times 100$ grid points is used. 37 points in the axial direction and 80 points in the spanwise direction are located on the wing. The minimum spacing at the surface is $\Delta z = 0.00001$ and a uniform spacing along the leading edge, $\Delta y = 0.00011$, is specified.

The numerical calculations for this case were found to be unsteady unless a coarse grid is employed. The unsteadiness in the calculations is attributed to a Kelvin-Helmholtz type instability of the shear layer which emanates from the leading edge of the delta wing and forming the primary vortex. This unsteady flow field is characterized by the formation and shedding of small-scale shear-layer vortical structures from the leading edge of the delta wing. It is suggested that this behavior is similar to that observed by Gad-el-Hak and Blackwelder in their water tunnel experiments [1].

A comparison of the average surface pressure at several axial locations along the wing with the experimental data of Hummel [22] is given in figure 5. The calculated results compare well with the experimental data showing only a slightly greater expansion in the region below the core of the primary vortex. The overprediction of the pressure at $x = 0.9$ is consistent with the calculations of Thomas [23] and is due in part to the onset of transition near the trailing edge in the experiment. Further details of these computations may be found in reference [8].

An investigation of the effect of time resolution on the unsteady behavior of the high Reynolds number case is carried out. Two values of Δt are considered, $\Delta t = 0.001$ and $\Delta t = 0.00025$. Three subiterations are used for each step at $\Delta t = 0.001$. The pressure is monitored at points traversed by the small scale vortices shed from the leading edge. Results for both time steps at an axial location $x = 0.3$ are given in figure 6. This location provided the highest computed frequency and should therefore be the most sensitive to time step resolution. The frequency for the smaller time step, $St \approx 24$, is higher than the frequency for the larger time step, $St \approx 20$. The basic nature of the flow remains the same, however. A time step of $\Delta t = 0.000125$ is chosen for subsequent calculations. This time step should provide adequate temporal

resolution, with approximately 300 time steps per cycle at the highest frequency. No subiterations are found to be necessary for this small time step.

5.2 Low Reynolds Number Case

Calculations are also made for a low Reynolds number, $Re = 50,000$. This provides several distinct advantages. First, the calculations are in the Reynolds number range of the experiments of Gad-el-Hak [1] and Lowson [6]. Better comparison of the computed results with experiment is then possible. Secondly, this lower value of Reynolds number also eliminates questions involving transition and turbulence that arise at the higher Reynolds number. Finally, the lower value of Reynolds number results in improved simulations for a given grid size.

The delta wing geometry itself is modelled as a flat plate. This is done to simplify the grid structure in the leading edge region of the delta wing. It is felt that the underside geometry has no significant effect on the flow physics being investigated.

Calculations for the lower value of Reynolds number are carried out on a $96 \times 151 \times 171$ grid. This grid contains 54 points in the axial direction and 80 points in the spanwise direction on the delta wing, with 133 points located above the delta wing. The minimum spacing at the wall is $\Delta z = 0.0001$ and the spacing along the leading edge of the delta wing varies from $\Delta y = 0.0005$ at the trailing edge to $\Delta y = 3.165 \times 10^{-5}$ at the apex. The spacing in the axial direction at the apex is $\Delta x = 0.01$ and at the trailing edge, $\Delta x = 0.003$. For the predominant portion of the wing there is a constant axial spacing of $\Delta x = 0.025$. This grid provides significant improvements in spatial resolution in all three coordinate directions.

The unsteadiness observed at high values of Reynolds number remains at $Re = 50,000$. The unsteady behavior of the flow field for this case is represented in figures 7 and 8. Each figure covers a time period corresponding to approximately one cycle of the unsteady behavior based on the frequency at the axial location, $x = 0.7$.

In figure 7 contours of the x-component of vorticity are shown for time $t = 0.4375$ to $t = 0.4875$ on cross planes located from 0.3 to 0.85. Positive values of vorticity are represented by the colors yellow, red, and magenta, with magenta representing the largest values. Negative values of vorticity are represented by the colors blue, cyan, and green with blue representing the smallest values. Clearly visible in the picture is the primary vortex over the delta wing. Also visible are a series of distinct small-scale vortical structures in the shear layer which emanates from the leading edge of the delta wing. These three-dimensional, vortical

structures are first evident in the flow at an axial location $x \approx 0.3$. The small-scale vortices consist of a coherent structure that forms first nearer the apex of the delta wing. The structure does not extend initially as a single vortex over the whole length of the leading edge of the delta wing. As the vortex sheds nearer the apex of the delta wing new parts of the vortical structure are forming further downstream. When the vortex sheds, it is convected around the primary vortex and its strength is dissipated. This process proceeds much more rapidly nearer the apex of the delta wing where the scale of the primary vortex is smaller. As the previous vortex is shed a new vortex is formed to take its place. The temporal evolution of this process is seen in figure 7. These small-scale vortices are believed to be the source of the striations observed by Gad-el-Hak, figure 1, and also observed by Lowson [6] in his smoke flow visualizations.

Further insight into the unsteady behavior may be obtained by looking at the evolution of the vortical structure for a typical cross plane, $x = 0.7$, figure 8. In this figure contours of the axial component of vorticity are plotted with blue contours being positive and red contours being negative. At time $t = 0.425$, the cycle begins with a small scale vortex starting to form. As time progresses from $t = 0.4375$ to $t = 0.4625$, this vortex grows in size and strength. Subsequently, for $t = 0.4625$ to $t = 0.4875$ the small-scale vortex is shed. The vortex convects around the primary vortex and is dissipated. During this process of shear-layer roll up and vortex shedding an interaction can be observed with the secondary region of vorticity. Vorticity of the opposite sign is shredded from this region and is dissipated along with the small-scale vortex as it is convected along the primary vortex. Even though contours of vorticity may not be compared directly to smoke flow visualizations, these figures appear to agree qualitatively with those of Lowson, figure 2.

A time history of the pressure at points in the flow field where the passing of the small-scale vortices may be monitored is made at several axial locations. A typical time history for the axial location $x = 0.7$ is given in figure 9. A dominant frequency is clearly seen even though the existence of other harmonics is evident. This dominant frequency is found to correspond to the shedding of the small-scale vortical structures. While the time histories are not sufficiently long to allow for an accurate frequency domain analysis, an average dominant frequency at each location can be found, and the results are shown in figure 10. The average frequencies are seen to scale almost linearly with axial distance.

The effect of the unsteady behavior on the surface pressure is shown for axial location $x = 0.7$, figure 11. The shedding of the small-scale vortices contributes to only a small temporal variation of the surface pressure outboard of the core of the primary vortex. This contrasts with the high Reynolds number case [8] where a marked temporal effect on the surface pressure outboard of the core of the primary vortex was seen. For the high Reynolds number the small-scale vortices form and are shed from the leading edge of the delta wing. In the low Reynolds number case the small-scale vortices form further away from the

leading edge of the delta wing, thus their interaction with the secondary separation region and with the flow near the surface of the wing is reduced. Time histories of the lift and drag coefficients also show only a slight temporal variation, figures 12 and 13. The lift coefficient varies by approximately 2.5% and the drag coefficient varies by approximately 1.8%. This temporal variation occurs at a much lower frequency than the shedding frequency of the small-scale vortices.

A typical simulated surface oil flow pattern for the delta wing is given in figure 14. A rather extensive region of reversed flow is seen outboard of the secondary separation line. This reversed flow region extends to nearly the midchord of the delta wing in an area located between the secondary and tertiary lines of separation. The three-dimensional extent of this reversed flow region is seen in figure 15 where the surface of zero x-component of velocity is plotted. From this figure it is seen that the largest region of reversed flow is located between the 75% chord location and the trailing edge. The reversed flow region extending forward to approximately midchord is only a small tertiary separation region near the surface of the delta wing.

6. Discussion

The current calculations show some similarities to the flow visualizations of both Gad-el-Hak and Blackwelder [1] and Lowson [6]. Direct comparison of the computations with experiments remains difficult, however, and only qualitative observations are possible. The majority of the results of Lowson, for example, are subject to a 50 Hz wind-tunnel background excitation which is not modelled in the computations. Furthermore, comparisons of vorticity contours with both smoke and dye flow visualizations are not exact and can sometimes be misleading [24]. Finally, the experiments and the computations are all done for different sweep angles. With these cautions noted the following observations can be made.

Both Gad-el-Hak and Lowson view the instability as a series of vortices formed and shed from the leading edge of the delta wing at a single frequency. Gad-el-Hak gives an empirical relation for this frequency:

$$St = \frac{1625}{\sqrt{Re}} \tag{6.1}$$

while Lowson gives the relation:

$$St = \frac{2577}{\sqrt{Re}} \tag{6.2}$$

This description of the instability is not completely consistent with what is observed in the calculations, however. Here the small-scale vortices do not form at the leading edge but further along the vortex sheet. Furthermore, the vortices do not roll up as a single unit along the entire length of the leading edge, but rather form first nearer the apex of the delta wing and then subsequently farther back along the leading edge of the wing. In the case of the experiments of Lowson this difference in character may be attributable to the 50 Hz wind-tunnel excitation of the flow field forcing the vortices to form at the leading edge.

Rather than a single frequency, an almost linear variation of the frequency of formation of the small-scale vortices is observed, with higher frequencies nearer the apex of the delta wing. For $Re = 50,000$, the empirical formula of Gad-el-Hak, equation (6.1) predicts a frequency, $St = 7.2$ while Lowson's relation, equation (6.2) predicts a frequency, $St = 11.5$. These values are of the same order as the frequencies computed in the aft portion of the delta wing. This gives confidence that the computed frequencies are not out of line with the actual physical situation.

Further insight into the shear-layer instability is obtained by considering an inviscid, linear stability analysis for a two-dimensional shear layer between co-flowing streams. Monkewitz and Huerre [25] have considered analytically the case where the mean velocity profile is described by:

$$U(y) = 1 + \lambda \tanh(\frac{y}{2}) \tag{6.3}$$

11

where $\lambda = (\Delta U/2\overline{U})$ is a measure of the velocity difference across the layer with $\overline{U}$ the average velocity of the two streams and $y = 4y^*/\delta_\omega$, where y^* is the dimensional length and δ_ω is the vorticity thickness. For $\lambda = 1$ the maximum amplified frequency from the linear spatial stability analysis was found to be $\omega = 0.21$ where:

$$\omega = \frac{\delta_\omega}{4} \frac{(2\pi f)}{\overline{U}} \qquad (6.1)$$

This value does not depend strongly on λ.

In an individual cross-plane at a given time, the flow which emanates from the leading edge of a delta wing may be viewed as a skewed shear layer. This shear layer may be separated into two components, an axial component in the x-direction and a shear or cross-flow component. To a first approximation the stability of the shear component is assumed to be the dominant factor in the stability of the shear layer. If the shedding frequencies at the cross-planes previously considered are nondimensionalized as in equation (6.1), values of ω are obtained in the range $\omega \approx 0.13-0.32$ with the specific value of ω dependent on the local shear-layer properties at the location chosen for nondimensionalization. These values of ω are of the same order as the maximum amplified frequency $\omega = 0.21$ found in the spatial stability analysis. Furthermore, a value of $\omega \approx 0.21$ always occurs at the approximate location where the small scale vortices are forming in the shear layer. This simplified analysis indicates that the computed flow field unsteadiness results from a shear-layer instability. Furthermore, the observed frequencies are consistent with a two-dimensional, spatial, linear stability analysis for these types of shear-layer flows.

Pairing of the small-scale vortical structures has been observed in both the experiments of Gad-el-Hak and Lowson. Gad-el-Hak suggests that the primary vortex over the delta wing originates as a series of pairings of the smaller scale vortices shed from the leading edge of the delta wing. Pairing of the small vortices is not observed in the computations. The reason for this discrepancy is not fully understood. The shear layer which emanates from the wing leading edge is expected to be highly susceptible to modification due to external excitation, intentional or unintentional. This excitation of the shear layer could promote the pairing process and is currently not modelled in the computations. In order to obtain a rigorous comparison of computations with experiment, a known forcing frequency might be required in both experiment and computation. The effect on the pairing process due to numerical dissipation in the calculations is also not fully understood, and requires further investigation.

It should also be noted that both experiments [26] and computations [27] for flow over slender bodies of revolution at large incidence exhibit a similar type of shear-layer instability. Small scale, three-dimensional vortices are observed to move along the primary surface of crossflow separation emanating from the body. The high frequency phenomenon observed is distinct from the von Karman-type shedding that occurs at

very high incidence for s ender bodies of revolution. The experiments [26] and computations [27] compare only qualitatively, but the numerical calculations capture the physical instability.

Finally, computations for the same delta wing and flow properties have been performed by others using several different numerical techniques [23,28,29]. These computations all show good agreement with the experimental measurements. No unsteady flow behavior similar to the instability previously discussed is reported in these references, however. Murman [30] has observed an unsteady flow behavior that results in a lack of convergence of the residual to steady state for Euler calculations over delta wings. The source of the lack of convergence is traced to the existence of unsteady, small-scale vortices in the shear layer from the wing leading edge. Since the computations are not fully time accurate, these observations are only qualitative. A full understanding of the effect of numerical technique, grid topology, and grid resolution on the computation of this type of shear-layer instability will require further investigations.

7. Conclusions

A numerical investigation of the unsteady vortex structure over a 76° sweep delta wing at 20.5° angle of attack has been carried out. Calculations are performed for a Mach number 0.2, and a Reynolds number 50,000. The numerical calculations show that the shear layer which emanates from the leading edge of the delta wing is subject to a Kelvin-Helmholtz type instability. Small-scale, three-dimensional vortical structures are observed in the shear layer. The small-scale vortices consist of a coherent structure that forms first nearer the apex of the delta wing and subsequently farther aft along the leading edge. These vortices are shed and convected around the primary vortex with their strength being dissipated. The frequency of shedding of these small-scale structures is seen to vary nearly linearly with axial location. The observed frequencies are consistent with the maximum amplified frequency found from an inviscid, linear, spatial stability analysis for a two-dimensional, cross-flow shear layer. The small-scale vortical structures have been shown to be related qualitatively to those observed by Gad-el-Hak [1] and Lowson [6] in their flow visualization experiments, though some differences in the specific character of the computed and experimental structures have been noted.

8. Nomenclature

C_p = pressure coefficient

E_t = total energy

f = frequency

J = transformation Jacobian

L = root chord length

M_∞ = freestream Mach number

p = pressure

Pr = Prandtl number

Re = Reynolds number

St = Strouhal number $St = fL/u_\infty$

t = nondimensional time $t = \bar{t}u_\infty/L$

u, v, w = velocity components in x, y and z

x, y, z = physical coordinates

y_e = location of leading edge

ξ, η, ζ = computational coordinates

δ_ω = vorticity thickness

ρ = density

μ = viscosity coefficient

ω = nondimensional frequency

$\tau_{i,j}$ = stress tensor

9. References

[1] Mohamed Gad-el-Hak and Ron F. Blackwelder. The Discrete Vortices from a Delta Wing. *AIAA Journal*, 23(6):961-962, June 1985.

[2] Garry L. Brown and Anatol Roshko. On Density Effects and Large Structure in Turbulent Mixing Layers. *Journal of Fluid Mechanics*, 64:775-816, 1974.

[3] C. D. Winant and F. K. Browand. Vortex Pairing: the Mechanism of Turbulent Mixing-Layer Growth at Moderate Reynolds Number. *Journal of Fluid Mechanics*, 63:237-255, 1974.

[4] F.M. Payne, T. T. Ng, R. C. Nelson, and L. B. Schiff. Visualization and Wake Surveys of Vortical Flow over a Delta Wing. *AIAA Journal*, 26(2):137-143 February 1988.

[5] F. M. Payne, T.T. Ng, R.C. Nelson, and L.B. Schiff. Visualization and Flow Surveys of the Leading Edge Vortex Structure on Delta Wing Planforms. AIAA-86-0330, January 1986.

[6] Martin V. Lowson. The Three Dimensional Vortex Sheet Structure on Delta Wings. In *Fluid Dynamics of Three-Dimensional Turbulent Shear Flows and Transition*, October 1988. AGARD-CP-438.

[7] J.F. Campbell, J.R. Chambers, and C. L. Rumsey. Observation of Airplane Flowfields by Natural Condensation Effects. *Journal of Aircraft*, 26(7):593-604, July 1989.

[8] Raymond E. Gordnier and Miguel R. Visbal. Unsteady Navier-Stokes Solutions for a Low Aspect Ratio Delta Wing. AIAA-90-1538, June 1990.

[9] Thomas H. Pulliam and Joseph L. Steger. Implicit Finite-Difference Simulation of Three-Dimensional Compressible Flows. *AIAA Journal*, 18(2):159-167, February 1980.

[10] Richard M. Beam and Richard F. Warming. An Implicit Factored Scheme for the Compressible Navier-Stokes Equations. *AIAA Journal*, 16, April 1978.

[11] Antony Jameson, Wolfgang Schmidt, and Eli Turkel. Numerical Solutions of the Euler Equations by Finite Volume Methods Using Runge-Kutta Time-Stepping Schemes. AIAA-81-1259, 1981.

[12] Miguel R. Visbal. Numerical Investigation of Laminar Juncture Flows. AIAA-89-1873, June 1989.

[13] W. Phillip Webster and Joseph S. Shang. Comparison Between Thin-Layer and Full Navier-Stokes Simulations Over a Supersonic Delta Wing. AIAA-90-0589, January 1990.

[14] Micheal J. Stanek and Miguel R. Visbal. Investigation of Vortex Development on a Pitching Slender Body of Revolution. AIAA-91-3273, September 1991.

[15] Miguel R. Visbal. Structure of Laminar Juncture Flows. *AIAA Journal*, 29(8):1273 1282, August 1991.

[16] Robert W. MacCormack. A Numerical Method for Solving the Equations of Compressible Viscous Flow. *AIAA Journal*, 20(9):1275-1281, September 1982.

[17] Man Mohan Rai and Sukumar R. Chakravarthy. An Implicit Form for the Osher Upwind Scheme. *AIAA Journal*, 24(5):735-743, May 1986.

[18] L. Bruce Simpson and David L. Whitfield. A Flux-Difference Split Algorithm for Unsteady Thin-Layer Navier-Stokes Solutions. AIAA-89-1995-CP, June 1989.

[19] Arthur C. Taylor III, Wing-fai Ng, and Robert W. Walters. Upwind Relaxation Methods for the Navier-Stokes Equations Using Inner Iterations. AIAA-89-1954-CP, June 1989.

[20] David L. Whitfield. Three-Dimensional Unsteady Euler Equation Solutions using a Flux Vector Splitting. Short Course on Numerical Grid Generation at Mississippi State University, June 1984.

[21] Dietrich Hummel. Study of the Flow Around Sharp-Edged Slender Delta Wings with Large Angles of Attack. NASA TT F-15,107, September 1973.

[22] Dietrich Hummel. On the vortex formation over a slender wing at large angles of incidence. In *High Angle of Attack Aerodynamics*, October 1978. AGARD-CP-247.

[23] James L. Thomas, Sherrie L. Krist, and W. Kyle Anderson. Navier-Stokes Computations of Vortical Flows Over Low Aspect Ratio Wings. *AIAA Journal*, 28(2):205-212, February 1990.

[24] I. Gursul, D. Lusseyran, and D. Rockwell. On interpretation of flow visualization of unsteady shear flows. *Experiments in Fluids*, 9:257-266, 1990.

[25] Peter A. Monkewitz and Patrick Huerre. Influence of the Velocity Ratio on the Spatial Instability of Mixing Layers. *Physics of Fluids*, 25(7):1137-1143, July 1982.

[26] David Degani and Gregory G. Zilliac. Experimental Study of Nonsteady Asymmetric Flow Around and Ogive - Cylinder at Incidence. *AIAA Journal*, 28(1):642-649, April 1990.

[27] L. B. Schiff, David Degani, and Sharad Gavali. Numerical Simulation of Vortex Unsteadiness on Slender Bodies of Revolution at Large Incidence. AIAA-89-0195, January 1989.

[28] Osama A. Kandil and H. Andrew Chuang. Unsteady Delta-Wing Flow Computation Using an Implicit Factored Euler Scheme. *AIAA Journal*, 28(9):1589–1595, September 1990.

[29] John A. Ekaterinaris and Lewis B. Schiff. Vortical Flows over Delta Wings and Numerical Prediction of Vortex Breakdown. AIAA-90-0102, January 1990.

[30] Earll M. Murman and Arthur Rizzi. Applications of Euler Equations to Sharp Edge Delta Wings With Leading Edge Vortices. In *Applications of Computational Fluid Dynamics in Aeronautics*, April 1986. AGARD-CP-412.

Figure 1: Dye Sheet Visualization Showing Small-Scale Vortices for a 60° Sweep Delta Wing at 10° Angle of Attack [1]

Figure 2: Smoke Flow Visualization of Vortex over a 70° Sweep Delta Wing at 20° Angle of Attack [6]
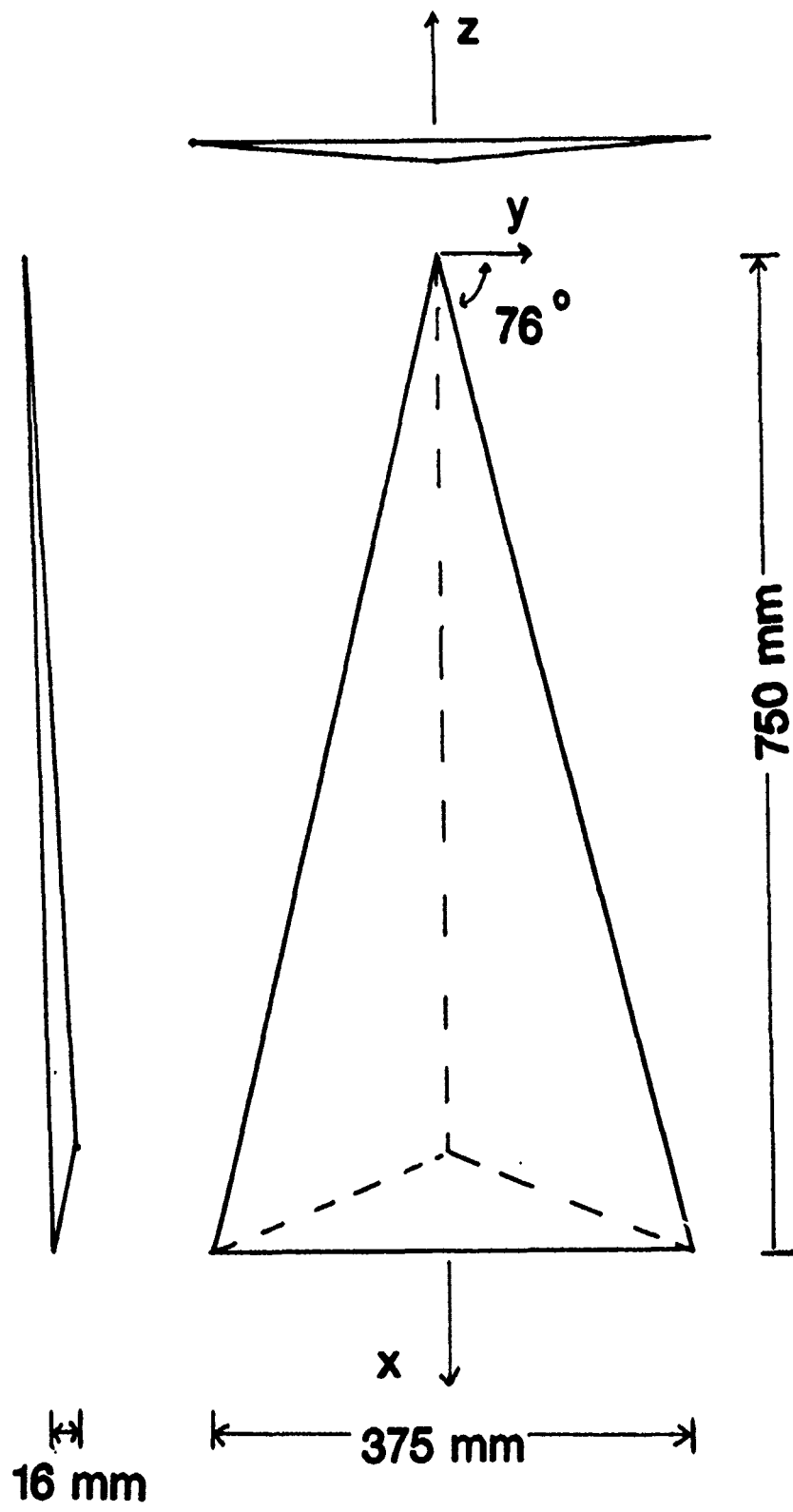
Figure 3: Delta Wing Configuration

21
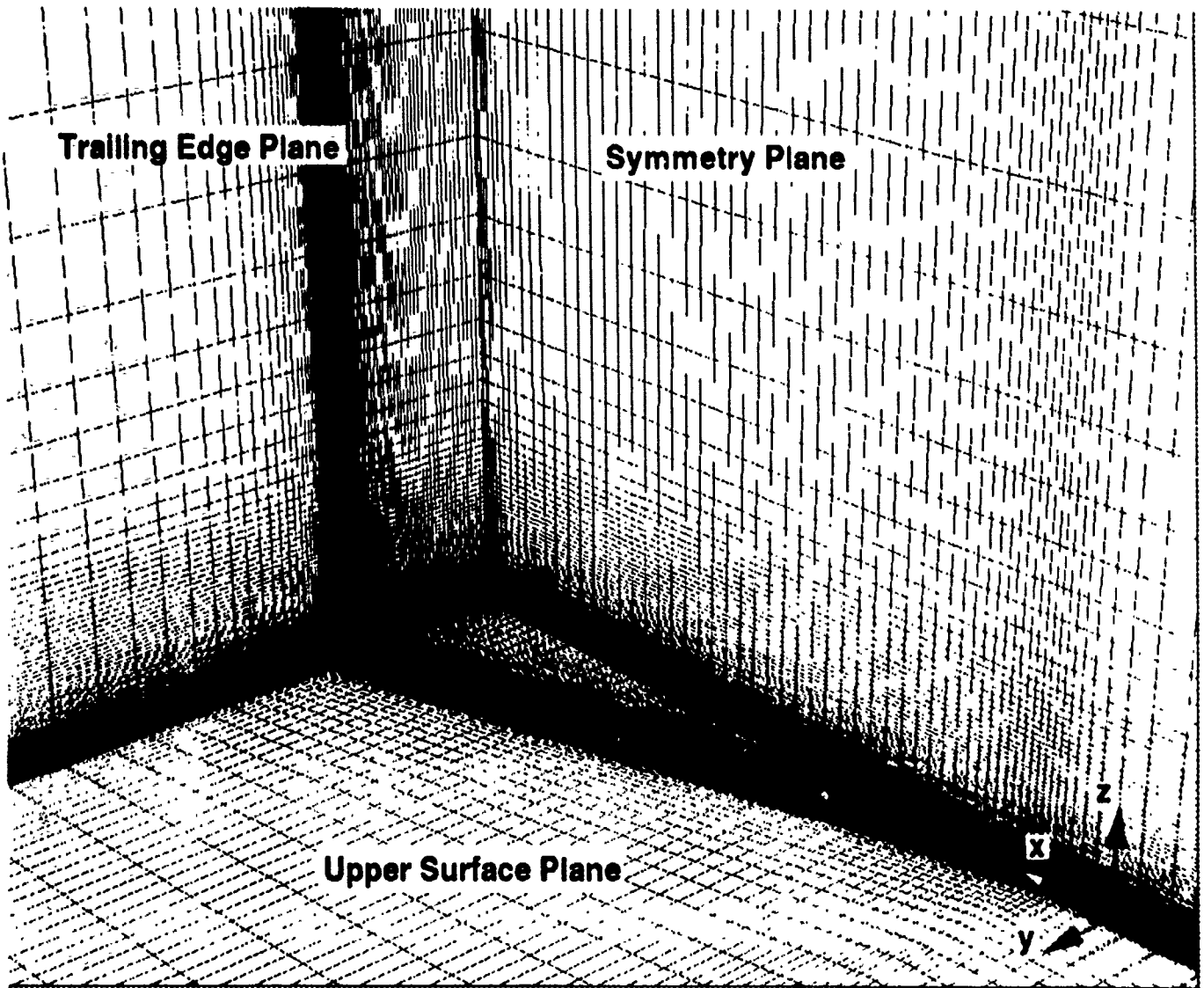
Figure 4: Grid Structure
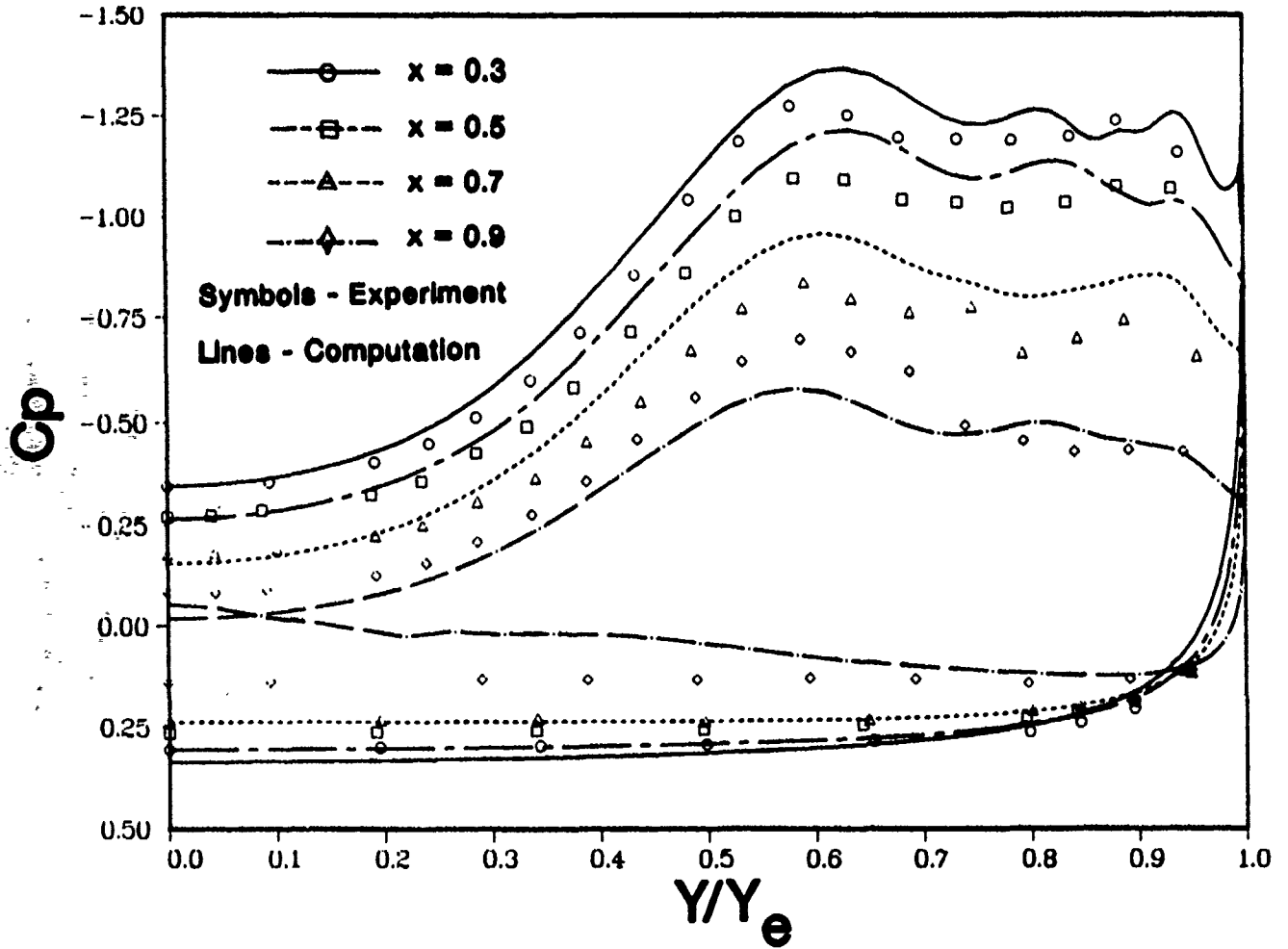
Figure 5: Comparison of Time-Averaged Surface Pressure with Experiment[21]:$\alpha = 20.5°$, $Re = 900,000$

23
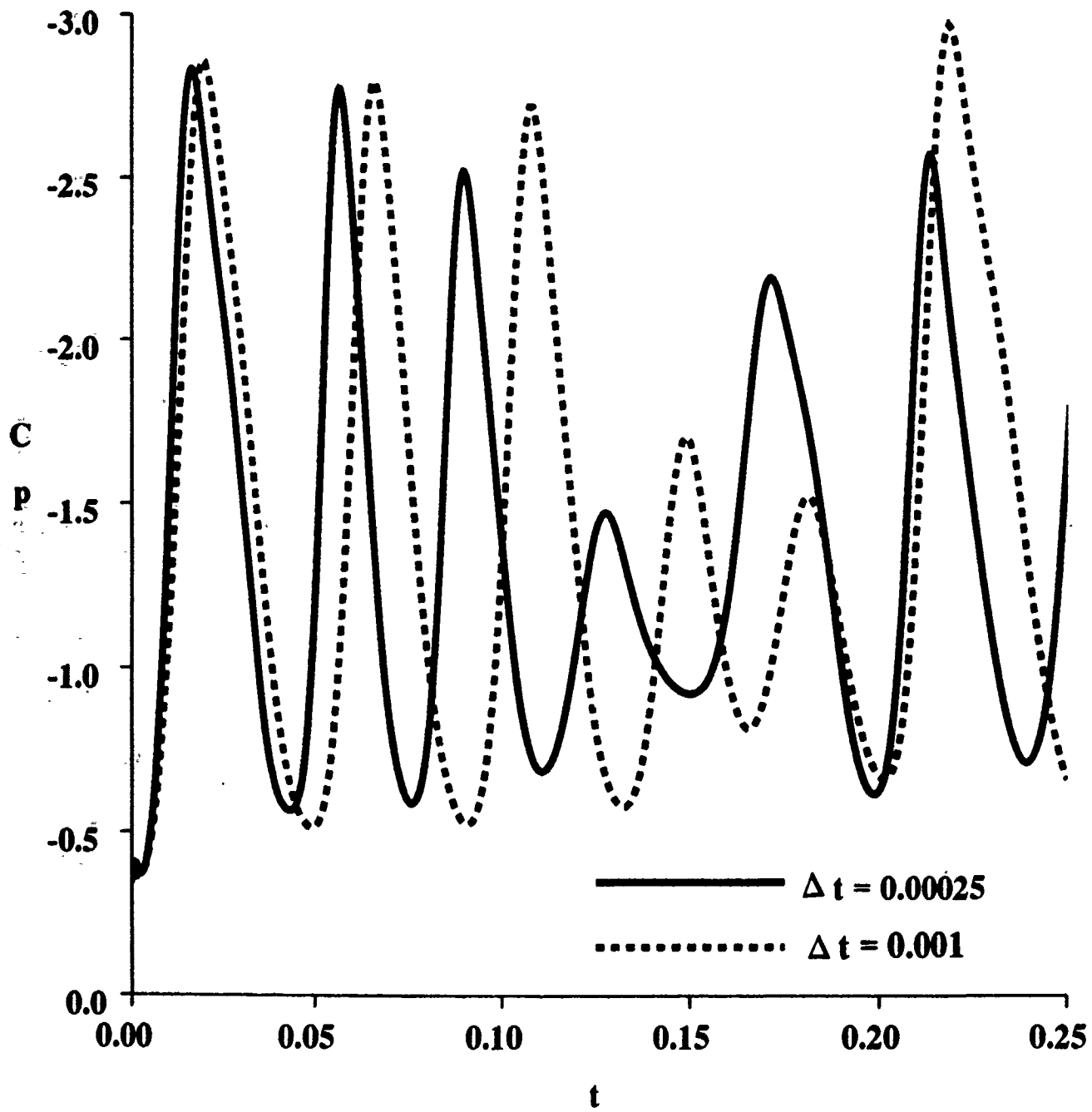
Figure 6: Comparison of the Time Histories of Pressure for Two Time Steps

24
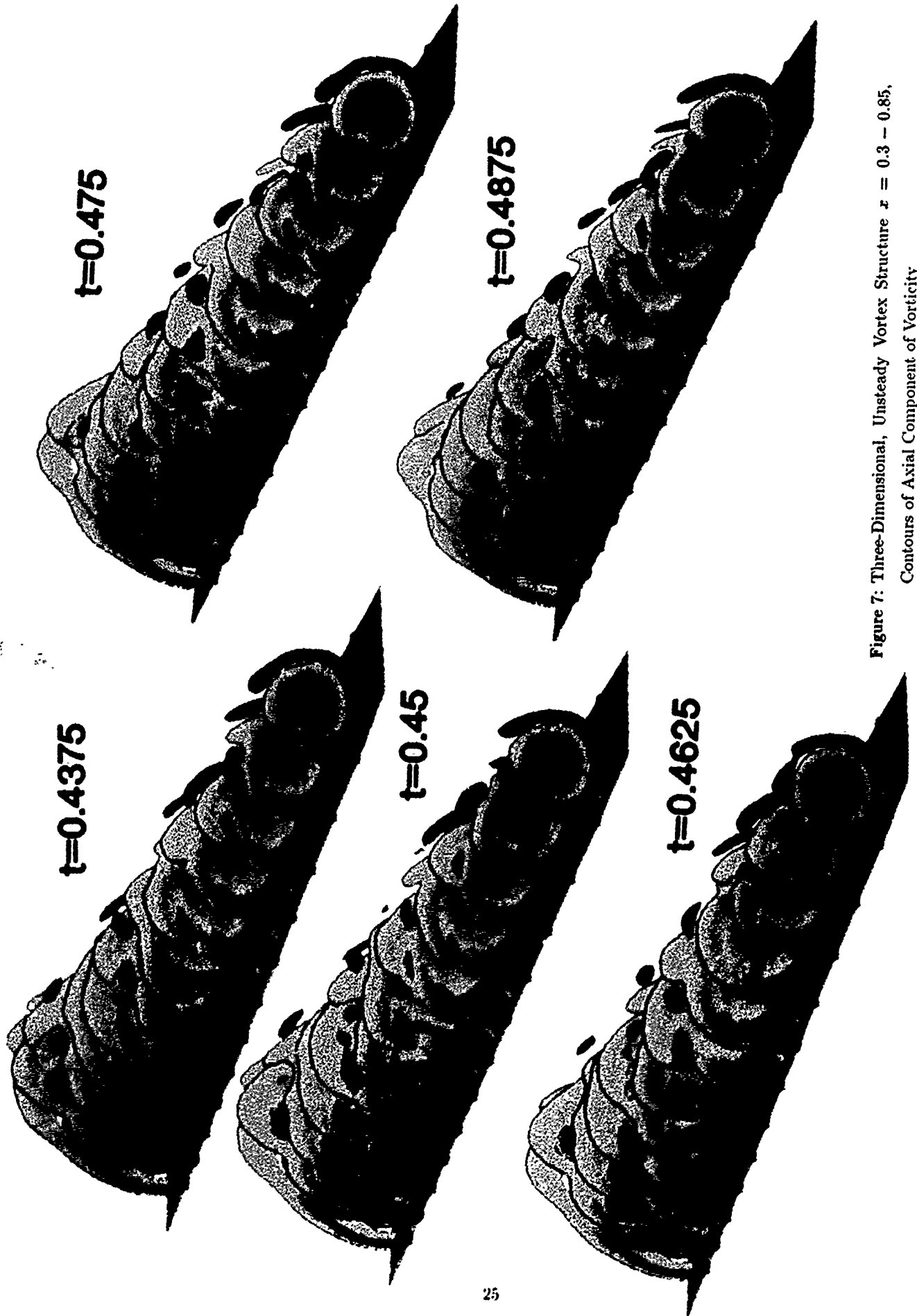
Figure 7: Three-Dimensional, Unsteady Vortex Structure $x = 0.3 - 0.85$, Contours of Axial Component of Vorticity

t=0.4375

t=0.45

t=0.4625

t=0.475

t=0.4875
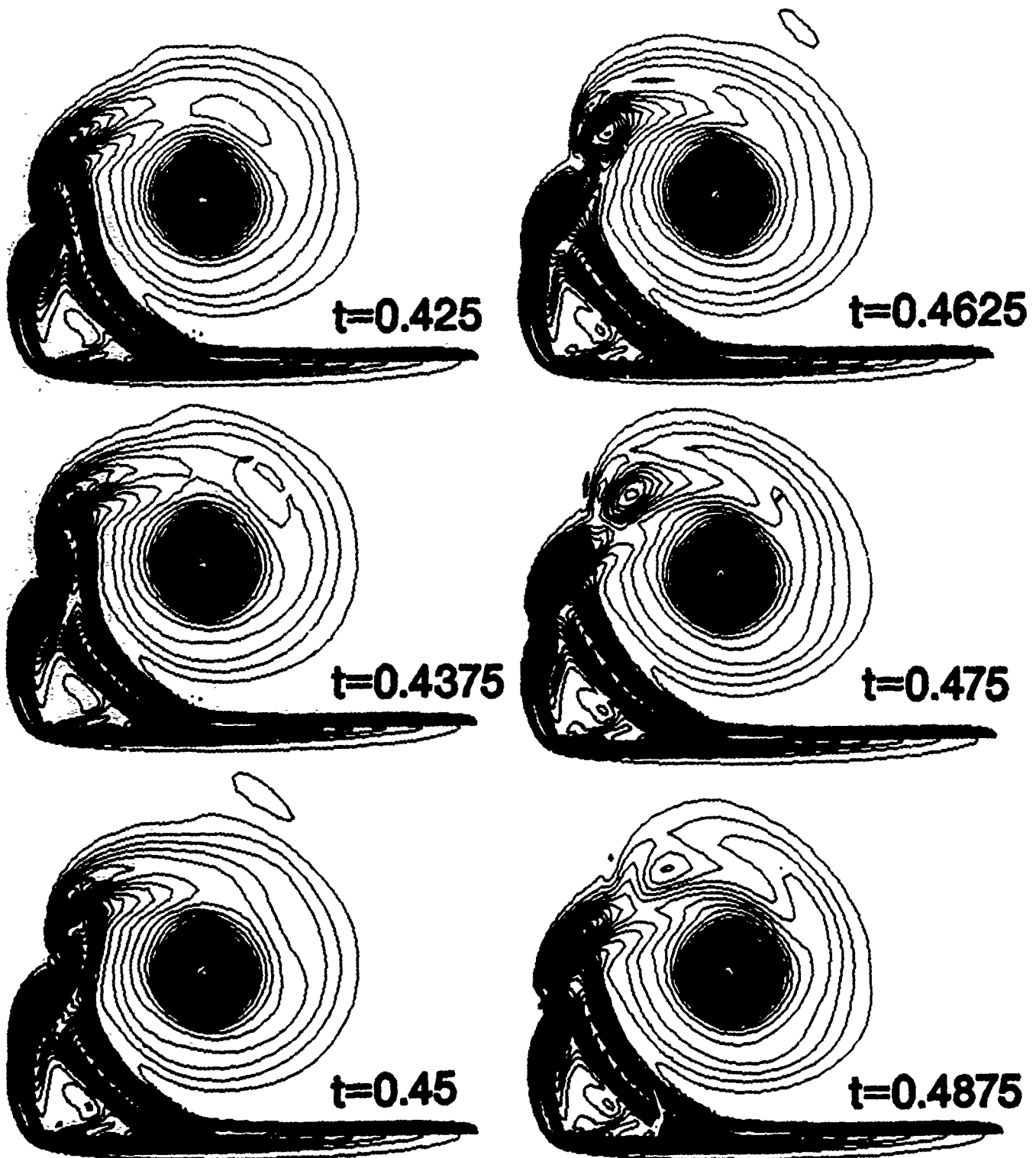
Figure 8: Unsteady Vortex Structure, $x = 0.7$, Contours of Axial Component of Vorticity: Blue > 0
Red < 0
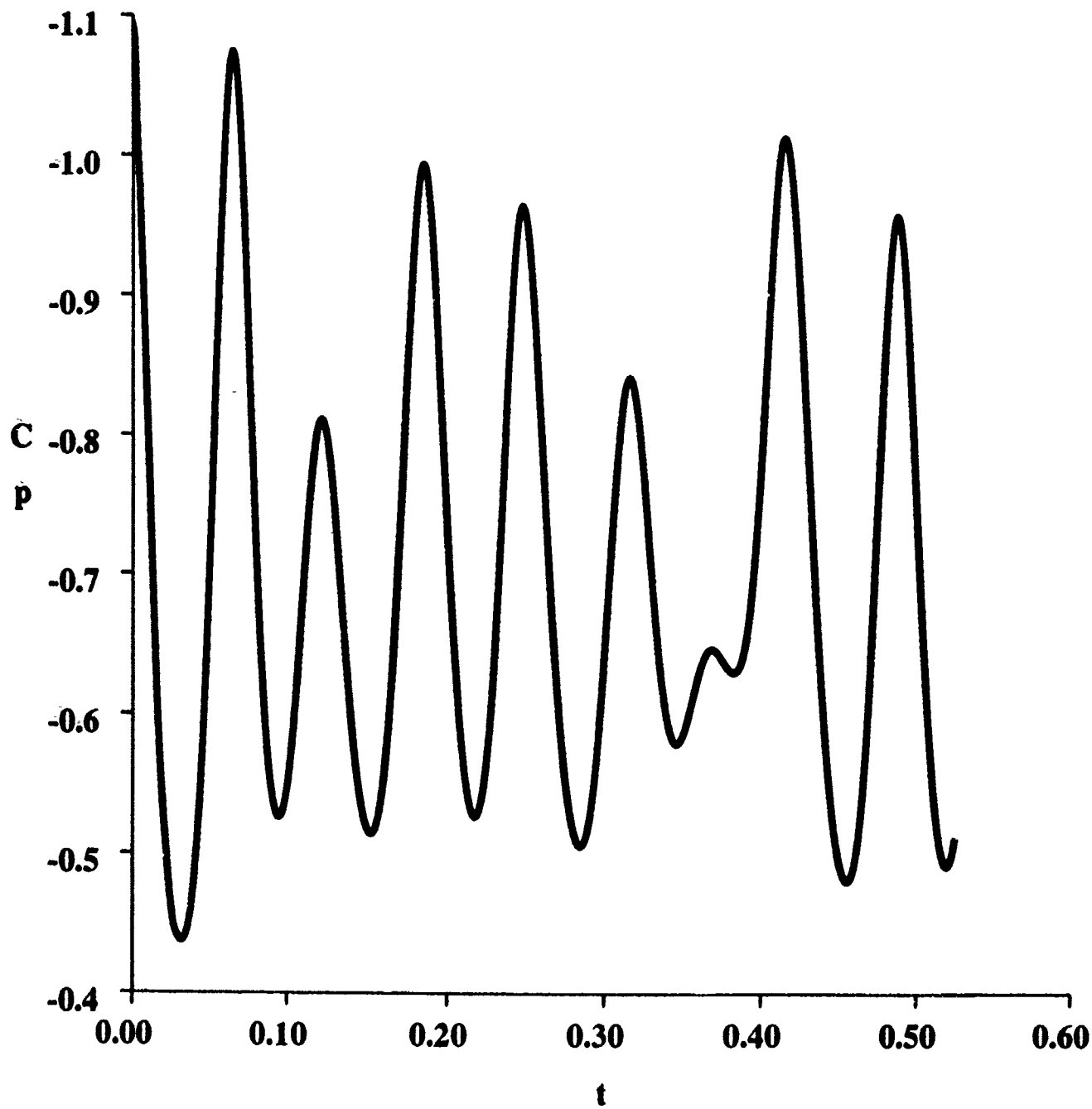
Figure 9: Typical Time History of Pressure for the Axial Location $x = 0.7$

St = f L / U∞

$$St = f L / U_\infty$$

Gad-el-Hak - St=7.2
Lowson - St=11.5
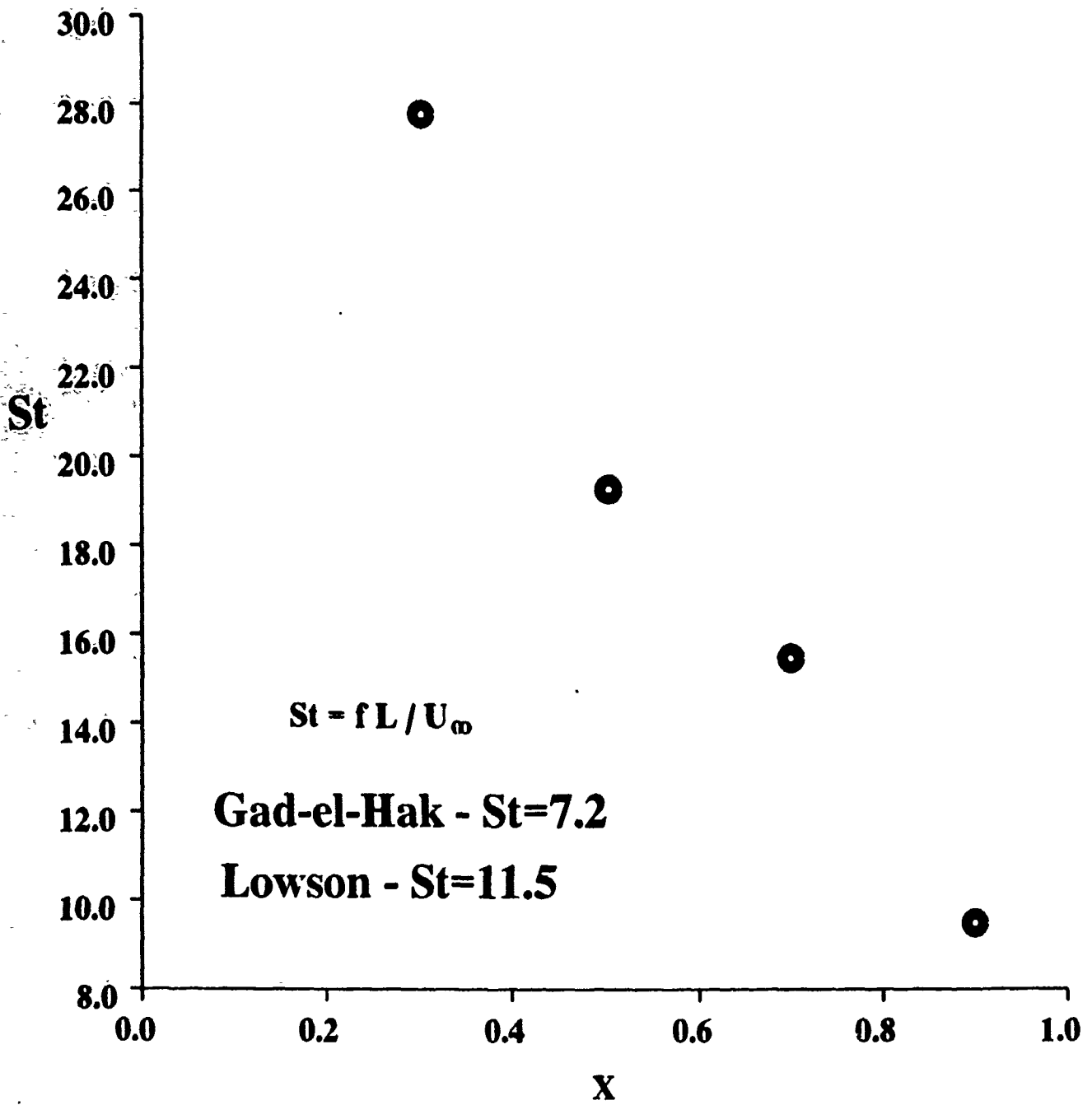
Figure 10: Shedding Frequency as a Function of Axial Location
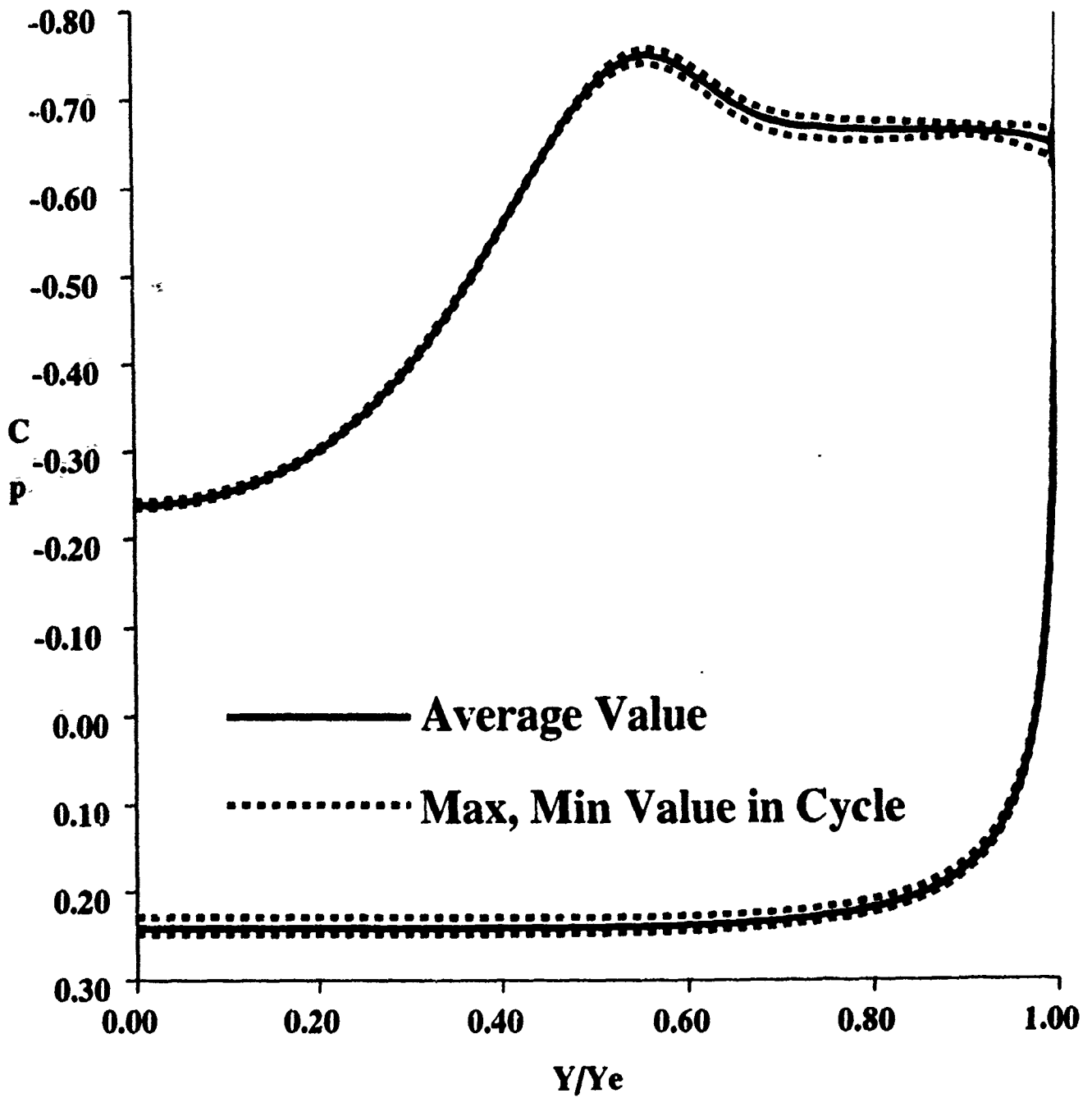
Figure 11: Comparison of Time-Averaged Surface Pressure with the Maximum and Minimum Values for One Cycle. $x = 0.7$
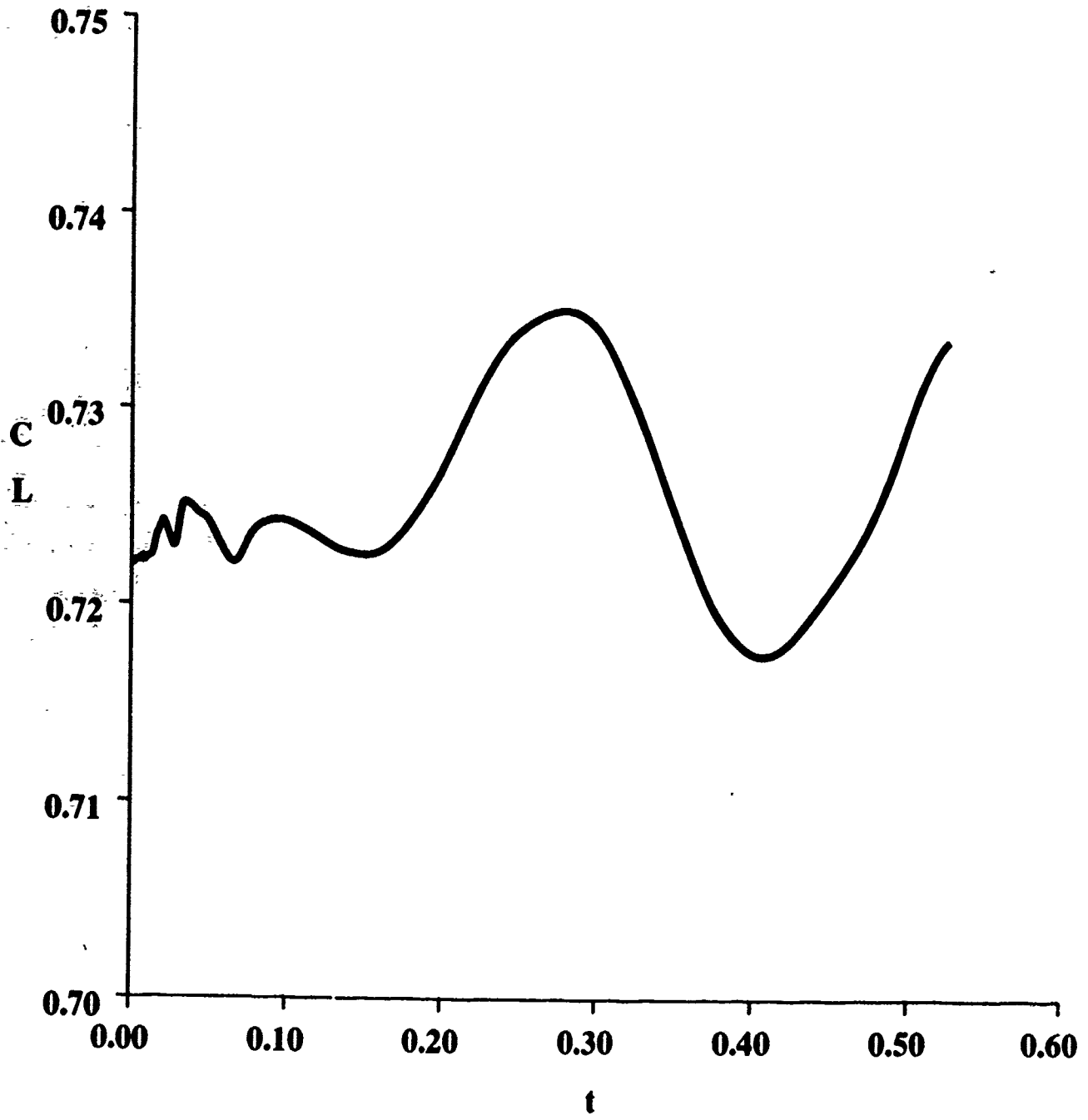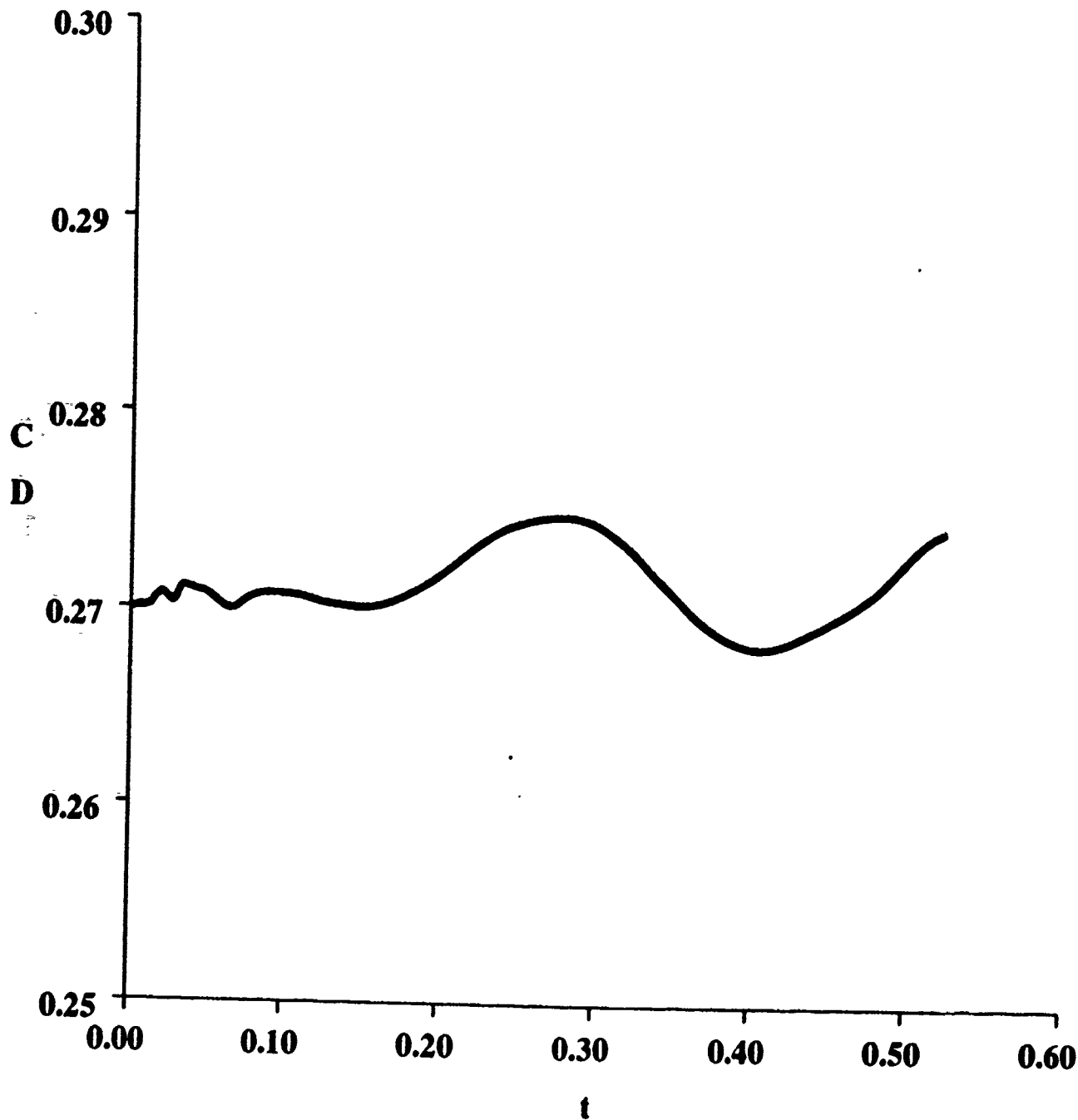
Figure 12: Time History of Lift Coefficient
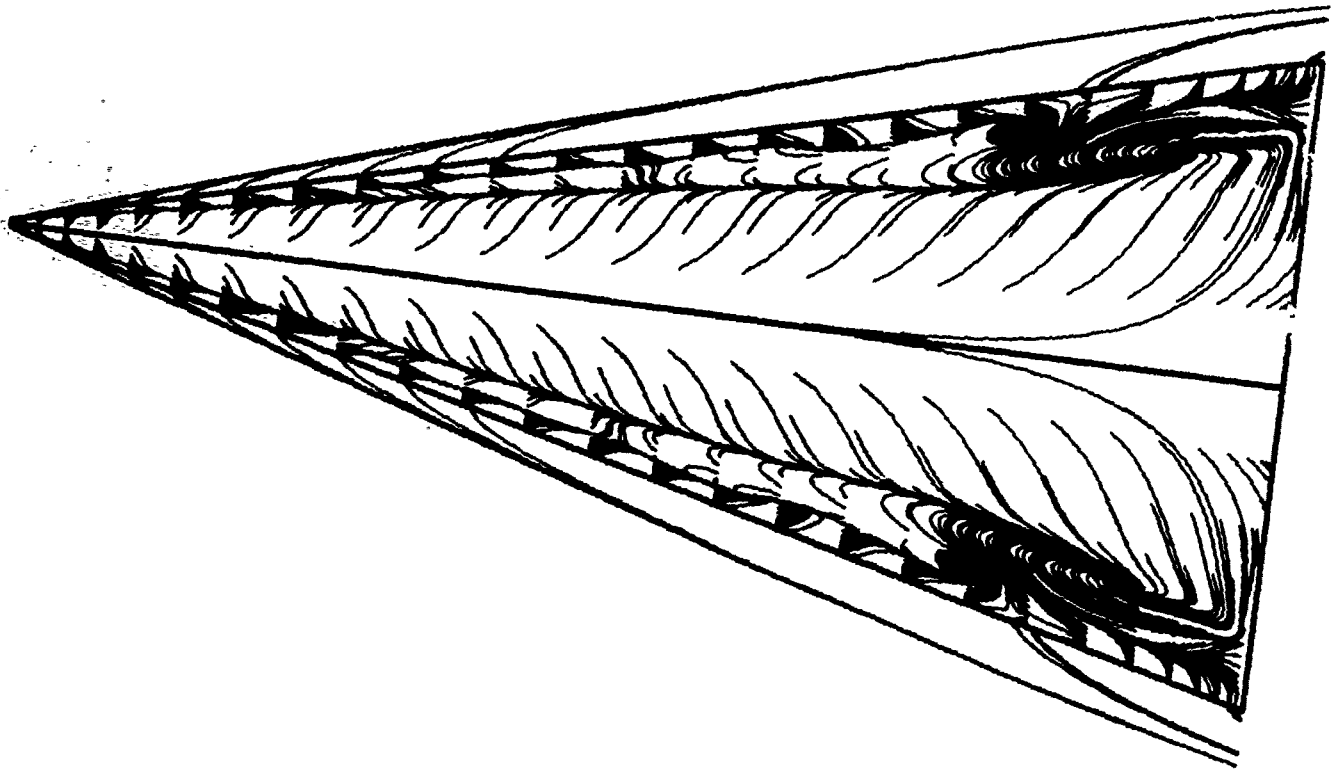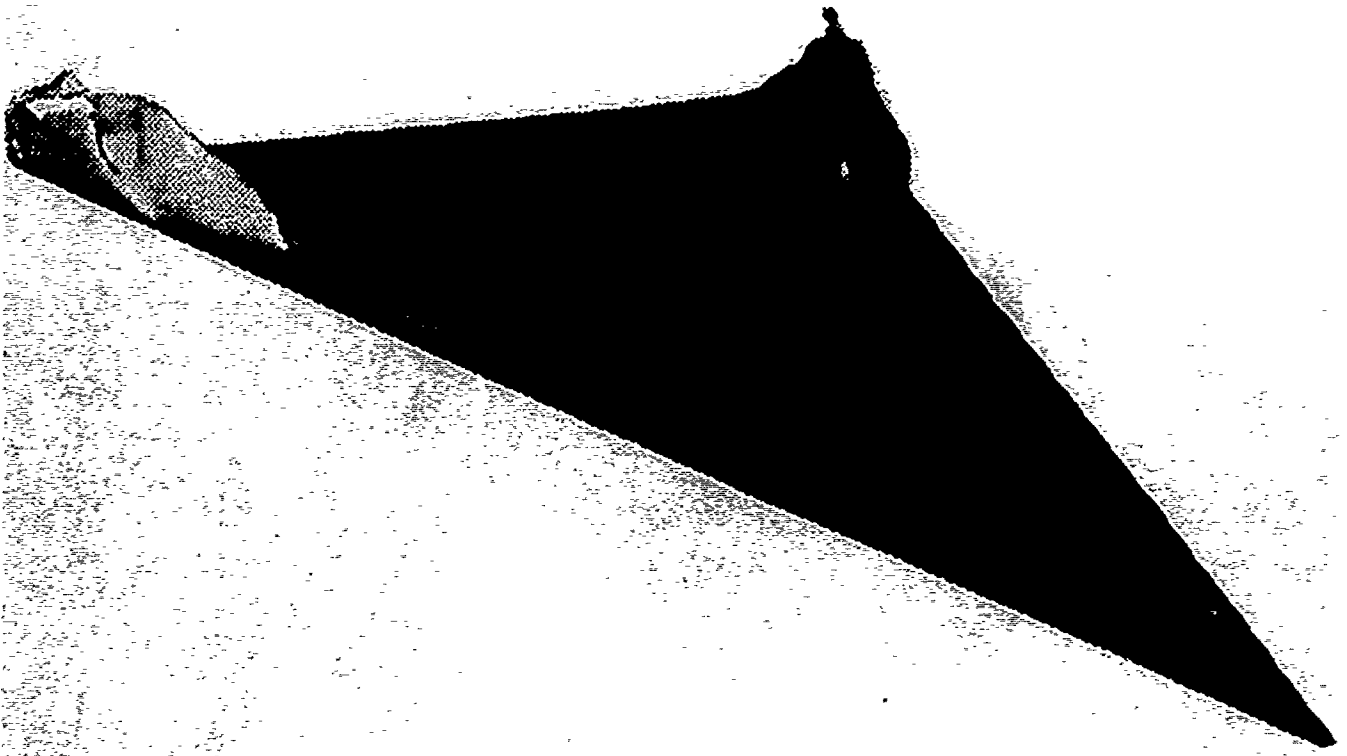
Figure 13: Time History of Drag Coefficient

Figure 14: Typical Simulated Surface Oil Flow Pattern. $t = 0.425$

32

Figure 15: Reversed Flow Region

33